Journal of Molecular Spectroscopy 270 (2011) 44–50

Contents lists available at SciVerse ScienceDirect

Journal of Molecular Spectroscopy

journal homepage: www.elsevier.com/locate/jms

Investigating the electronic states of BaOH by V-type double resonance spectroscopy and *ab initio* calculations: Further evidence of perturbation from the $\widetilde{A}'^2\Delta$ state

J.D. Tandy [a], J.-G. Wang [a], J. Liévin [b], P.F. Bernath [a,*]

[a] Department of Chemistry, University of York, Heslington, York YO10 5DD, United Kingdom
[b] Service de Chimie Quantique et Photophysique, Université Libre de Bruxelles, CPi 160/09, 50 av F.D. Roosevelt, B-1050 Bruxelles, Belgium

ARTICLE INFO

Article history:
Received 19 July 2011
In revised form 30 August 2011
Available online 8 September 2011

Keywords:
High-resolution
Laser excitation
BaOH
BaOD
V-type double resonance
Ab Initio

ABSTRACT

A single band belonging to the $\widetilde{A}'^2\Delta - \widetilde{X}^2\Sigma^+$ band system has been rotationally analyzed for each of the two isotopologues, BaOH and BaOD, using high-resolution V-type optical–optical double resonance spectroscopy. BaOH and BaOD molecules were synthesized in a Broida-type oven. High-resolution spectra were recorded by monitoring the dip in fluorescence of the $\widetilde{B}^2\Sigma^+ - \widetilde{X}^2\Sigma^+$ transition excited by a single-mode ring dye laser (pump laser), whilst a single-mode Ti:Sapphire laser scanned the corresponding $\widetilde{A}'^2\Delta - \widetilde{X}^2\Sigma^+$ transition. The observed spectra resemble a typical $^2\Pi-^2\Sigma$ transition, believed to emanate from single or triple quanta of the bending vibration in the $\widetilde{A}'^2\Delta$ state. Measured rotational lines have been assigned and rotational and fine structure parameters determined through a combined least-squares fit with the millimeter-wave pure rotational data of the $\widetilde{X}^2\Sigma^+$ state. Previous analyses of the $\widetilde{A}^2\Pi - \widetilde{X}^2\Sigma^+$ transitions of BaOH and BaOD yielded significantly different spin–orbit coupling constants, which were attributed to possible global and local perturbations arising from vibrationally-excited bands of the $\widetilde{A}'^2\Delta$ state. Although the newly observed $\widetilde{A}'^2\Delta$ state bands have not been conclusively assigned a specific spin state, the derived Ω-doubling constants show significant $^2\Pi_{1/2}$ character, further indicating strong interactions between the $\widetilde{A}^2\Pi$ and $\widetilde{A}'^2\Delta$ states of BaOH. To validate these conclusions, *ab initio* calculations have been carried out to further understand the nature of the BaOH excited states. The $\widetilde{D}'^2\Sigma^+$, $\widetilde{D}^2\Sigma^+$, $\widetilde{C}^2\Pi$, $\widetilde{B}^2\Sigma^+$, $\widetilde{A}^2\Pi$, $\widetilde{A}'^2\Delta$ and $\widetilde{X}^2\Sigma^+$ states have been characterized by means of multireference configuration interaction calculations using the MOLPRO software. Calculated vertical term energies show relatively good agreement with existing optical data.

1. Introduction

Previous spectroscopic analyses of the excited electronic states of BaOH have been somewhat limited but have all shown a degree of complexity and ambiguity [1–5]. The $\widetilde{D}^2\Sigma^+ - \widetilde{X}^2\Sigma^+$ and $\widetilde{C} - \widetilde{X}$ transitions of BaOH have been observed at relatively low-resolution by Pooley et al. in a supersonic expansion using laser ablation [1]. Two band systems exhibiting $^2\Pi-^2\Sigma^+$ character between ~20000 and 22000 cm^{-1} (tentatively named the $\widetilde{C} - \widetilde{X}$ spectral region of BaOH) were observed but unable to be assigned unambiguously. The apparent anomalous behavior of the $\widetilde{C}^2\Pi$ state was attributed to either Renner–Teller effects or a perturbing $^2\Delta$ state in close proximity. Kinsey-Nielsen et al. first published an analysis of the $\widetilde{B}^2\Sigma^+ - \widetilde{X}^2\Sigma^+$ transition that showed evidence of parity dependant perturbations from interactions with the $\widetilde{A}^2\Pi$ state [2]. The $\widetilde{A}^2\Pi - \widetilde{X}^2\Sigma^+$ and $\widetilde{A}'^2\Delta - \widetilde{X}^2\Sigma^+$ transitions were then investigated at low-resolution by Fernando et al. who tentatively assigned two bands at ~11784 and 11304 cm^{-1} to a stretching sequence of the $\widetilde{A}'^2\Delta_{5/2} - \widetilde{X}^2\Sigma^+$ transition [3]. We recently reported high-resolution analyses of the $\widetilde{A}^2\Pi(0\,0\,0) - \widetilde{X}^2\Sigma^+(0\,0\,0)$ transitions of BaOH and BaOD that yielded an unexpected and considerable difference between the two spin–orbit constants, A, for the $\widetilde{A}^2\Pi$ states of the two molecules [4,5]. This difference was suggested to result from strong global perturbations originating from the lower-lying $\widetilde{A}'^2\Delta$ state. These perturbations were also indicated by the apparent failure of the pure precession and unique perturber models in both BaOH and BaOD and the unrealistic r_0(OH) bond length, calculated from the B values of the $\widetilde{A}^2\Pi$ states.

A detailed examination of the $\widetilde{A}'^2\Delta$ state is now required to further understand the interactions between the low-lying electronic states of BaOH. Barrow and co-workers previously examined the $\widetilde{A}'^2\Delta$ state of the isoelectronic species BaF at low-resolution and found the vibrational levels to be interleaved with those of the $\widetilde{A}^2\Pi$ state [6]. It was also noted that the vibrational spacing in the $\widetilde{A}'^2\Delta$ state is of the same order as the spin–orbit splitting, potentially causing strong perturbations between the $^2\Delta_{5/2}$ and $^2\Delta_{3/2}$ spin components. The same group then examined six electronic excited states of BaF via high-resolution Fourier transform spectroscopy including the $\widetilde{A}'^2\Delta$ state. The following deperturbation analysis led

* Corresponding author. Fax: +44 1904 432516.
E-mail address: pfb500@york.ac.uk (P.F. Bernath).

0022-2852/$ - see front matter © 2011 Elsevier Inc. All rights reserved.
doi:10.1016/j.jms.2011.08.009

to large effects on the energies and spin–orbit coupling constants of the 5*d* states ($\widetilde{B}^2\Sigma^+, \widetilde{A}^2\Pi$ and $\widetilde{A}'^2\Delta$) [7,8]. Indeed, their prior investigations on BaH and BaD showed the corresponding 5*d* states formed a mutually perturbing triad [9]. It is therefore quite possible that these observations may also be true in the low-lying states of BaOH and thus a high-resolution analysis of the $\widetilde{A}'^2\Delta$ state should assist in verifying these predictions.

Ab initio calculations are also useful in the investigation of small metal-containing species [10–16]. In particular the use of complete active space self-consistent field (CASSCF) and multi-reference configuration interaction (MRCI) approaches has proved to be adequate for characterizing the excited-state electronic structure of such systems and for predicting their vertical term energies. A similar investigation of the excited electronic states of BaOH may therefore yield valuable information regarding the character of these states and the interactions between them.

The present paper reports our high-resolution study of two bands lying in the $\widetilde{A}'^2\Delta$ state spectral region of BaOH and BaOD using V-type optical–optical double resonance spectroscopy. Rotational and fine structure constants have been determined for both bands through a combined least-squares fit. Tentative assignments for the two bands are discussed with reference to potential perturbations with the close-lying $\widetilde{A}^2\Pi$ state. Calculated vertical term energies for the six lowest-lying excited electronic states ($\widetilde{D}'^2\Sigma^+$, $\widetilde{D}^2\Sigma^+$, $\widetilde{C}^2\Pi$, $\widetilde{B}^2\Sigma^+$, $\widetilde{A}^2\Pi$ and $\widetilde{A}'^2\Delta$) of BaOH are presented and compared to existing experimental data. Analyses of the singly occupied molecular orbital (SOMO) populations for each state are also discussed.

2. Experimental

BaOH and BaOD molecules were generated by the reaction of Ba metal vapor with H_2O_2 or D_2O vapor respectively in a Broida-type oven as described in our previous analyses [4,5]. A chemiluminescent flame from the production of either BaOH or BaOD molecules was observed at optimal oven conditions. Due to our photomultiplier tube (PMT) having poor sensitivity in the spectral region of interest it was not possible to scan the $\widetilde{A}'^2\Delta$ state directly using the laser excitation method previously utilized for the observation of the $\widetilde{A}^2\Pi(0\,0\,0) - \widetilde{X}^2\Sigma^+(0\,0\,0)$ transitions. V-type optical–optical double resonance spectroscopy is a useful alternative technique to avoid the sensitivity problem of the PMT when directly recording fluorescence from the near-infrared $\widetilde{A}'^2\Delta - \widetilde{X}^2\Sigma^+$ transition. In this technique a single-mode ring dye laser (Coherent 699-29, operating with pyridine II dye) was used to excited a specific rotational line of the $\widetilde{B}^2\Sigma^+ - \widetilde{X}^2\Sigma^+$ transition (pump laser) whilst a single-mode titanium:Sapphire laser (Coherent 899–29, probe laser) was used to scan the $\widetilde{A}'^2\Delta - \widetilde{X}^2\Sigma^+$ transition. Fig. 1 illustrates the use of V-type double resonance spectroscopy to study the $\widetilde{A}'^2\Delta_{3/2}(0\,1\,0, \Pi_{1/2})$ vibronic state (see Section 4) of BaOH, ignoring parity. Double resonance spectra were recorded as the dips in the fluorescence of the $\widetilde{B}^2\Sigma^+ - \widetilde{X}^2\Sigma^+$ transition induced by the depletion in the common ground state ($\widetilde{X}^2\Sigma^+$) whenever the scanning probe laser hit a corresponding line of the $\widetilde{A}'^2\Delta - \widetilde{X}^2\Sigma^+$ transition. Typical output powers of ~300 mW and ~200 mW were observed for the Ti:Sapphire and ring dye lasers, respectively.

The ring cavity dye laser output was first focussed vertically into the reaction chamber of the Broida oven and used to scan the $\widetilde{B}^2\Sigma^+ - \widetilde{X}^2\Sigma^+$ transition of either BaOH or BaOD to locate the required rotational lines. The PMT was used to collect the fluorescence signal through a 0.32 m monochromator employed as a band pass filter and set to the wavelength corresponding to the $\widetilde{B}^2\Sigma^+(0\,0\,0) - \widetilde{X}^2\Sigma^+(0\,0\,1)$ transition of either BaOH or BaOD. Phase sensitive detection was employed by using a mechanical chopper to modulate the pump laser beam and a lock-in amplifier to process the fluorescence signal from the PMT. Spectra were recorded in 5 cm^{-1} segments at a scan speed of 3 GHz per second with a data sampling interval of 50 MHz. The absolute frequency of the dye laser was calibrated by simultaneously recording the emission spectrum of an I_2 cell [17]. The rotational lines of the $\widetilde{B}^2\Sigma^+ - \widetilde{X}^2\Sigma^+$ transitions were identified by referring to the previous work of Kinsey-Nielsen et al. [2].

The dye laser was then used to pump specific rotational lines of the $\widetilde{B}^2\Sigma^+ - \widetilde{X}^2\Sigma^+$ transition whilst the Ti:S laser scanned through the resonant frequencies of the $\widetilde{A}'^2\Delta - \widetilde{X}^2\Sigma^+$ transition. All double resonance signals corresponding to rotational $\widetilde{A}'^2\Delta - \widetilde{X}^2\Sigma^+$ transitions with an identical J'' value in the common lower electronic state (i.e. the $\widetilde{X}^2\Sigma^+$ state) were observed as dips in the monitored $\widetilde{B}^2\Sigma^+ - \widetilde{X}^2\Sigma^+$ fluorescence. The overlap of the two laser beams was carefully adjusted to maximize any double resonance signal obtained. Spectra were recorded in 5 cm^{-1} segments at a scan speed of 1 GHz per second with a data sampling interval of 30 MHz. The absolute frequency of the titanium:sapphire laser was calibrated by simultaneously recording the absorption spectrum of a heated I_2 cell [17].

3. Results and analysis

3.1. V-type double resonance spectroscopy

Previous analyses of the $\widetilde{B}^2\Sigma^+$ states of BaOH and BaOD [2] were first utilized to locate the $\widetilde{B}^2\Sigma^+(0\,0\,0) - \widetilde{X}^2\Sigma^+(0\,0\,0)$ transitions, which were then scanned using the ring cavity dye laser. With these assignments it was possible to select specific $\widetilde{B}^2\Sigma^+(0\,0\,0) - \widetilde{X}^2\Sigma^+(0\,0\,0)$ rotational transitions to pump whilst the Ti:Sapphire laser scanned the spectral region of interest in an attempt to locate the corresponding rotational lines of an $\widetilde{A}'^2\Delta - \widetilde{X}^2\Sigma^+$ transition. The Ti:S laser was scanned as far as possible to the lower wavenumber side of the previously assigned $\widetilde{A}^2\Pi_{1/2} - \widetilde{X}^2\Sigma^+$ transitions of BaOH and BaOD [4,5], in order to locate any potentially observable states below the $\widetilde{A}^2\Pi_{1/2}$ sub-state. Using this method a single band was observed at ~11 306 cm^{-1} for BaOH. Similarly, a second band at ~11 283 cm^{-1} was observed for BaOD.

Rotational lines in corresponding *P*-, *Q*- and *R*-branches with identical J'' values to that of the pump transition were, in general, clearly observed with a good signal-to-noise ratio. In addition, a host of less intense rotational lines were also observed throughout the band, corresponding to transitions with J'' values in the vicinity of the pump transition. Fig. 2 shows a portion of the observed spectrum between 11302.5 and 11307.5 cm^{-1} when the dye laser was set to pump the R_1 J'' = 29.5 line in the $\widetilde{B}^2\Sigma^+ - \widetilde{X}^2\Sigma^+$ transition of BaOH. As illustrated, it was possible to observe both a strong single line corresponding to J'' = 29.5 and many weaker lines corresponding to J'' = 27.5, 28.5, 30.5, 31.5, etc. These weaker lines are thought to arise from a collisional redistribution of energy among levels in close proximity to the J'' = 29.5 level of the $\widetilde{X}^2\Sigma^+$ state. To confirm the fluorescence dips were truly double resonance signals, the Ti:S laser frequency was fixed on a strong dip and the signal was monitored whilst each laser was blocked in turn. The double resonance signal was extinguished by blocking either of the two laser beams.

Once the band had been fully scanned the frequency of the dye laser was tuned to other rotational lines of the $\widetilde{B}^2\Sigma^+ - \widetilde{X}^2\Sigma^+$ transition to extend the double resonance spectra in order to contain a reasonable range of J'' values. This process allowed a more comprehensive rotational line list to be extracted for each observed band. The bands observed for BaOH and BaOD both show structure of six rotational branches, closely mimicking a typical Hund's case (c) $^2\Pi$ – Hund's case (b) $^2\Sigma^+$ pattern with a 1*B* Q_{fe}/R_{ff} band head and the R_{ff}/Q_{fe} and P_{ee}/Q_{ef} pairs of branches [18]. In total 152 and 187 lines

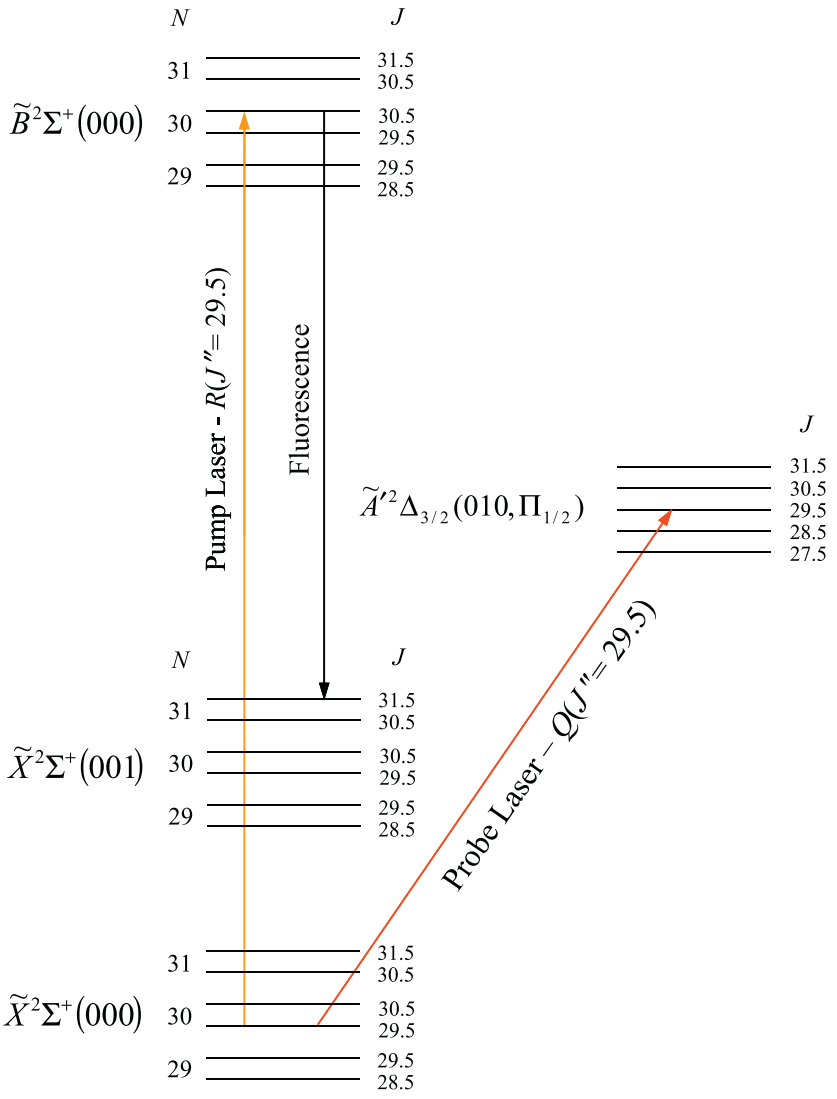

Fig. 1. Examining the $\widetilde{A}'^2\Delta_{3/2}(0\,1\,0, \Pi_{1/2})$ vibronic state of BaOH using V-type double resonance spectroscopy. The affect of parity in each vibronic state has been ignored for clarity. The pump laser excites the $R(J'' = 29.5)$ $\widetilde{B}^2\Sigma^+(0\,0\,0) - \widetilde{X}^2\Sigma^+(0\,0\,0)$ rotational transition of BaOH, whilst the probe laser scans the corresponding $Q(J'' = 29.5)$ $\widetilde{A}'^2\Delta_{3/2}(0\,1\,0, \Pi_{1/2}) - \widetilde{X}^2\Sigma^+$ rotational transition. A dip in the monitored $\widetilde{B}^2\Sigma^+(0\,0\,0) - \widetilde{X}^2\Sigma^+(0\,0\,1)$ emission is observed due to the depletion in the common ground state ($\widetilde{X}^2\Sigma^+$).

were rotationally assigned for the bands of BaOH and BaOD respectively. Term values for the excited states of the observed bands were expressed in the Hund's case (c) expression:

$$F(J) = BJ(J+1) - D[J(J+1)]^2 + H[J(J+1)]^3 + L[J(J+1)]^4 \pm 1/2(J+1/2)[p + p_D(J+1/2)^2 + p_H(J+1/2)^4 + p_L(J+1/2)^6], \quad (1)$$

where B, D, H and L are rotational constants and p, p_D, p_H and p_L are Ω-doubling constants, were performed for the excited states. The ±sign in Eq. (1) refers to the e- (+) and f-parity (−) levels, respectively.

A combined least-squares fit was performed for each band including the optical data of this work and 47 and 24 pure rotational lines of the $\widetilde{X}^2\Sigma^+$ states of BaOH and BaOD respectively [19,20]. Each line in the fit was weighted according to its experimental uncertainty. An estimated uncertainty of 10^{-6} cm^{-1} was applied for the millimeter-wave data [19,20], while the optical data (this work) used an uncertainty of 0.005 cm^{-1}. Table 1 lists the spectroscopic constants generated from the least-squares fit with the transitions modeled as the Hund's case (c) $^2\Pi$ – Hund's case (b) $^2\Sigma^+$ for BaOH and BaOD. The measured lines for both observed bands of BaOH and BaOD are provided as Supplementary material from this journal.

3.2. Ab initio calculations

Ab initio calculations were carried out to determine vertical term energies and orbital populations of the six lowest lying excited electronic states of BaOH. The procedure was based upon prior *ab initio* investigations by Ram et al. on diatomic transition metal species [10–16]. This first involved a preliminary optimization of the molecular orbitals via a state-averaged CASSCF calculation [21] involving nine electrons distributed into an active orbital space of seven σ, three π and one δ orbitals, arising from the 5d, 6s, 6p and 7s orbitals of barium, the 2s and 2p orbitals of oxygen and the 1s orbital of hydrogen. These orbitals were then used in an internally contracted MRCI calculation (CMRCI) [22] in which all electrons of the active space were correlated. All CMRCI energies were corrected for Davidson's contribution for four-particle unlinked clusters [23].

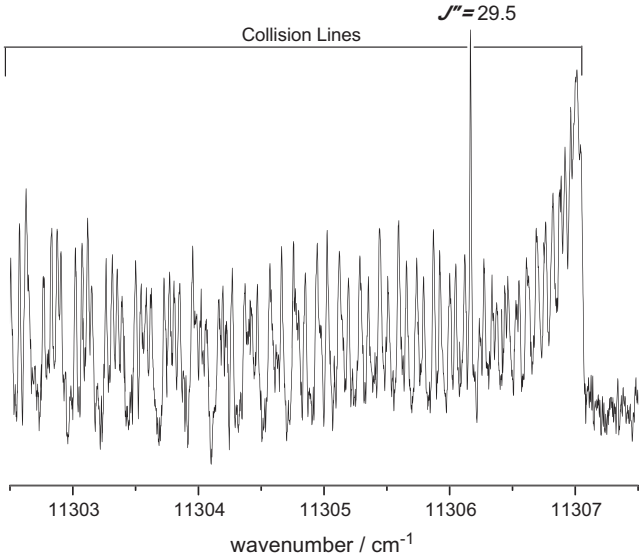

Fig. 2. A portion of the V-type double resonance spectrum between 11302.5 and 11307.5 cm^{-1}. The spectrum was recorded by scanning a single-mode ring titanium:Sapphire laser across the spectral region of interest with a single-mode ring cavity dye laser set to pump the $R_1J'' = 29.5$ line in the $\widetilde{B}^2\Sigma^+ - \widetilde{X}^2\Sigma^+$ transition of BaOH. The PMT was used to collect the fluorescence signal through a 0.32 m monochromator employed as a band pass filter and set to the wavelength corresponding to the $\widetilde{B}^2\Sigma^+(0\,0\,0) - \widetilde{X}^2\Sigma^+(0\,0\,1)$ transition of BaOH. The lock-in amplifier was used to flip the signal phase 180° to give a positive reading for every dip in the $\widetilde{B}^2\Sigma^+(0\,0\,0) - \widetilde{X}^2\Sigma^+(0\,0\,1)$ fluorescence. Both a strong single line corresponding to $J'' = 29.5$ and many weaker lines, thought to arise from a collisional redistribution of energy among the lower common state ($\widetilde{X}^2\Sigma^+$) levels, were observed. The band shows evidence of six rotational branches, closely mimicking a typical Hund's case (a) $^2\Pi$ – Hund's case (b) $^2\Sigma^+$ pattern with a $1BQ_{fe}/R_{ff}$ band head and the R_{ff}/Q_{fe} and P_{ee}/Q_{ef} line pairs.

The majority of previous experimental data indicate that the excited states of BaOH are linear [1–5] and therefore the molecular bond angle was fixed at 180° throughout the procedure. A fully relativistic pseudopotential developed by Stoll et al. was used to describe the 46 core electrons of the Ba atom [24], together with corresponding valence quadruple zeta basis sets [24] augmented by polarization orbitals on each atom (up to *g*-type functions). Dunning's aug-cc-PVQZ basis sets [25,26] were used to describe the oxygen and hydrogen atoms in order to provide a balanced valence description of all atoms. The size of the CASSCF (CMRCI) wavefunctions was ~455 000 (42 526 000) configuration state functions in C_{2v} symmetry. All calculations were performed with the MOLPRO software package [27].

The equilibrium geometry of the ground state was first derived at the CMRCI level of theory, by means of numerical gradient searches. The optimized values of the Ba–O and O–H internuclear distances are 2.270 Å and 0.955 Å respectively. Energies for the six lowest lying excited electronic states of BaOH calculated at this geometry provide vertical term energies, which are compared to those observed by experiment in Table 2. The main configurations in the CMRCI wavefunctions for each state and their corresponding weights (squares of the configuration interaction coefficients) are also listed. The excited state configurations are characterized by single excitations with respect to the $\widetilde{X}^2\Sigma^+$ ground state configuration. According to atomic populations (see Table 3), orbitals 6σ to 9σ adiabatically correlate with the 6*s*, $5d\sigma$, 7*s* and $6p\sigma$ atomic orbitals of barium respectively. Orbitals 3π and 4π correlate to $6p\pi$ and $5d\pi$ respectively, whilst orbital 1δ correlates to $5d\delta$. The relative barium *s*, *p*, and *d* orbital populations of the seven lowest-lying electronic states of BaOH were also determined by a Mulliken population analysis of the natural orbitals of the CMRCI wavefunctions and are summarized in Table 3.

4. Discussion

4.1. The $\widetilde{A}'^2\Delta$ state

The identification of the two $^2\Pi$ bands observed in the spectroscopic analysis of this work requires some attention. Electronically forbidden $^2\Delta - ^2\Sigma^+$ transitions in linear triatomic molecules may become allowed through vibronic coupling with the v_2 bending mode, as explained by Jarman and Bernath in their investigation of the $\widetilde{C}^2\Delta$ state of CaOH [28]. By coupling the vibrational angular momentum *l* associated with the Ba–O–H bending mode with the electronic angular momentum Λ, $^2\Delta - ^2\Sigma^+$ transitions involving $\Delta v_2 = \pm1, \pm3$, etc. become allowed while the origin band remains forbidden. If Renner–Teller interactions are ignored the inclusion of a single quanta of the bend in the $\widetilde{A}'^2\Delta$ state should give rise to a vibronic state of $^2\Pi$ character. Electronic transitions from this vibronic state to the $\widetilde{X}^2\Sigma^+$ state of BaOH should therefore be allowed and readily observable.

The $\widetilde{A}'^2\Delta_{3/2}$ sub-state of BaOH may also interact with the higher-lying $\widetilde{A}^2\Pi_{3/2}$ sub-state by spin–orbit coupling. The magnitude of this interaction may be roughly estimated by calculating the one-electron atomic spin–orbit matrix element $(1/2\zeta\hat{l}_- \cdot \hat{s}_+)$ coupling the $5d\delta_{+2}\beta$ and a $5d\pi_{+1}\alpha$ spin–orbitals of the $\widetilde{A}'^2\Delta_{3/2}$ and $\widetilde{A}^2\Pi_{3/2}$ sub-states, using an atomic orbital approximation. When using a value of 380 cm^{-1} for ζ for the 5*d* orbital of Ba^+ [29], the magnitude of this spin–orbit interaction was calculated to be 380 cm^{-1}. This procedure neglects the considerable barium $6p\pi$ character of the $\widetilde{A}^2\Pi$ state and Franck–Condon factors, but nevertheless indicates a significant off-diagonal spin–orbit interaction between the $\widetilde{A}^2\Pi$ and $\widetilde{A}'^2\Delta$ states of BaOH.

In our previous analysis of the $\widetilde{A}^2\Pi$ state a discrepancy was detected in the spin–orbit coupling parameters for BaOH and BaOD [5]. It was suggested that a $^2\Pi_{1/2}$ vibronic state originating from

Table 1
Spectroscopic constants (in cm^{-1}) for BaOH and BaOD[a].

Constant	BaOH		BaOD	
	$\widetilde{X}^2\Sigma(0\,0\,0)$[b]	$^2\Pi$[b]	$\widetilde{X}^2\Sigma(0\,0\,0)$[b]	$^2\Pi$[b]
T	0.0	11306.28772(70)	0.0	11283.20086(50)
B	0.2166090279(95)	0.2129610(19)	0.19575190(11)	0.19208717(98)
$D \times 10^{-7}$	1.642757(83)	2.188(13)	1.26339(73)	1.5846(37)
$\gamma \times 10^{-3}$	2.37952(50)		2.1754(26)	
$\gamma_D \times 10^{-9}$	7.5(38)			
p		0.217340(91)		0.147231(37)
$p_D \times 10^{-6}$		−1.51(11)		−2.974(19)

[a] Values in parentheses are 1σ standard deviation, in units of the last significant digits.
[b] Constants generated by a combined fit of the $\widetilde{A}'^2\Delta_{3/2}(0\,1\,0, \Pi_{1/2}) - \widetilde{X}^2\Sigma^+$ transition data and the millimeter-wave data of the $\widetilde{X}^2\Sigma^+$ state [20] using the Hund's case (c) expression, $F(J) = BJ(J+1) - D[J(J+1)]^2 + H[J(J+1)]^3 + L[J(J+1)]^4 \pm 1/2(J+1/2)[p + p_D(J+1/2)^2 + p_H(J+1/2)^4 + p_L(J+1/2)^6]$.

Table 2
Vertical term energies (in cm^{-1}) for the excited states of BaOH.

Electronic state	CMRCI[a]	Experiment	Main configuration	Weight[f] (%)
$\widetilde{X}^2\Sigma^+$	0	0	$1\sigma^2 2\sigma^2 3\sigma^2 1\pi^4 4\sigma^2 5\sigma^2 2\pi^4 6\sigma^1$	75.9
$\widetilde{A}'^2\Delta$	9885	$\leqslant$11306.2877[b]	$6\sigma \rightarrow 1\delta$	85.5
$\widetilde{A}^2\Pi$	11688	11763.2363[c]	$6\sigma \rightarrow 3\pi$	72.3
$\widetilde{B}^2\Sigma^+$	13127	13200.024[d]	$6\sigma \rightarrow 7\sigma$	67.9
$\widetilde{C}^2\Pi$	20393	~20438[e]	$6\sigma \rightarrow 4\pi$	66.2
$\widetilde{D}^2\Sigma^+$	23699	~23057[e]	$6\sigma \rightarrow 8\sigma$	71.6
$\widetilde{D}'^2\Sigma^+$	26213	–	$6\sigma \rightarrow 9\sigma$	67.1

[a] Calculated at the CMRCI equilibrium geometry of the ground electronic state (see text).
[b] Value taken from the single band of BaOH observed in this work.
[c] Ref. [4].
[d] Ref. [2].
[e] Term energies based upon low-resolution band heads of Ref. [1].
[f] Squares of the configuration interaction coefficients.

Table 3
Barium atomic orbital populations in seven electronic states of BaOH[a].

	$\widetilde{X}^2\Sigma^+$	$\widetilde{A}'^2\Delta$	$\widetilde{A}^2\Pi$	$\widetilde{B}^2\Sigma^+$	$\widetilde{C}^2\Pi$	$\widetilde{D}^2\Sigma^+$	$\widetilde{D}'^2\Sigma^+$
$s\sigma$	2.95	1.92	1.92	1.92	1.92	2.75	2.20
$p_z(p\sigma)$	2.03	1.96	1.96	2.25	1.95	2.12	2.87
$p_x(p\pi)$	1.96	1.96	2.64	1.96	2.29	1.96	1.96
$p_y(p\pi)$	1.96	1.96	1.96	1.96	1.96	1.96	1.96
p_{total}	5.95	5.88	6.56	6.17	6.20	6.04	6.78
$d_{z2}(d\sigma)$	0.11	0.10	0.10	0.70	0.10	0.12	0.24
$d_{xz}(d\pi)$	0.07	0.07	0.36	0.07	0.79	0.07	0.07
$d_{yz}(d\pi)$	0.07	0.07	0.07	0.07	0.02	0.07	0.07
$d_{x2-y2}(d\delta)$	0.02	1.00	0.02	0.02	0.02	0.07	0.07
$d_{xy}(d\delta)$	0.02	0.02	0.02	0.02	0.02	0.02	0.02
d_{total}	0.29	1.26	0.57	0.88	1.00	0.30	0.42

[a] Calculated from Mulliken populations of the natural orbitals of the CMRCI wavefunctions of the different electronic states. The *z*-axis is defined as the molecular axis of BaOH.

the $\widetilde{A}'^2\Delta$ electronic state of BaOH may lie in close proximity to the $\widetilde{A}^2\Pi_{1/2}$ state and that the mixing of these states could cause strong global perturbations. The term values for the two observed $^2\Pi$ bands shown in Table 1 both lie within 180 cm^{-1} of their corresponding $\widetilde{A}^2\Pi_{1/2}$ state origins (~11483 cm^{-1} and 11431 cm^{-1} for BaOH and BaOD respectively) [5], indicating that they may be the predicted perturbing vibronic states. Table 1 also shows that the $^2\Pi$ bands for both BaOH and BaOD require relatively large *p* values (an Ω-doubling parameter) in the least-squares fit. Λ-doubling is known to be small in most Δ states [30] and the observed parameters are in fact more comparable to those observed for the $\widetilde{A}^2\Pi_{1/2}$ states (~0.146 and 0.179 cm^{-1} for BaOH and BaOD respectively) [5]. This demonstrates strong $^2\Pi_{1/2}$ character in the two observed states and is a further indication of strong interactions with the corresponding $\widetilde{A}^2\Pi_{1/2}$ states of BaOH and BaOD.

It is of course possible that the newly observed bands actually originate from the $\widetilde{A}^2\Pi_{1/2}$ states of BaOH and BaOD and the bands previously assigned to these sub-states originate from a lower lying $\widetilde{A}'^2\Delta_{3/2}(\Pi_{1/2})$ vibronic state. This assignment seems unlikely however as the spin–orbit coupling parameter of the $\widetilde{A}^2\Pi$ states would be significantly larger ($A \approx 737$ cm^{-1} and 753 cm^{-1} for BaOH and BaOD, respectively) than the corresponding value for BaF ($A \approx 632$ cm^{-1}) [7]. As the original values for *A* derived in the previous laser excitation investigation [4,5] are considerably closer to that of BaF (~560 cm^{-1} and 606 cm^{-1} for BaOH and BaOD respectively), it seems more probable that the observed bands of this study are $\Pi_{1/2}$ vibronic states originating from the $\widetilde{A}'^2\Delta$ electronic states of BaOH and BaOD. Furthermore, the vibronic coupling of a $^2\Delta_{3/2}$ state with $l = 1$ (vibrational angular momentum) yields vibronic states of $^2\Pi_{1/2}$ and $^2\Phi_{5/2}$, whilst a $^2\Delta_{5/2}$ state generates $^2\Pi_{3/2}$ and $^2\Phi_{7/2}$ vibronic states [31]. The observed $\widetilde{A}'^2\Delta(\Pi_{1/2})$ bands should therefore originate from the $\widetilde{A}'^2\Delta_{3/2}$ sub-states of BaOH and BaOD.

As the corresponding $\widetilde{A}'^2\Delta_{5/2}(\Pi_{3/2})$ bands were not observed in this investigation, the term value *T* and spin–orbit coupling constant *A* could not be determined for the $\widetilde{A}'^2\Delta$ state of BaOH or BaOD. The vibrational assignment of the two observed $\widetilde{A}'^2\Delta_{3/2}(\Pi_{1/2})$ bands is therefore more challenging. The vibrational band previously observed at ~11307 cm^{-1} by Fernando et al. was assigned to the $\widetilde{A}'^2\Delta_{5/2}(0\,0\,0) - \widetilde{X}^2\Sigma^+(0\,0\,0)$ transition of BaOH [3]. However, the observations of this study would suggest that this band actually originates from the $\widetilde{A}'^2\Delta_{3/2}$ sub-state and exhibits vibronic coupling with a single quantum of the bending vibration of BaOH. A more likely vibrational assignment would therefore be the $\widetilde{A}'^2\Delta_{3/2}(0\,1\,0, \Pi_{1/2}) - \widetilde{X}^2\Sigma^+(0\,0\,0)$ transition of BaOH. This conclusion is further justified as no other $^2\Pi - \widetilde{X}^2\Sigma^+$ transitions were observed to the red side of this band. The small difference between the *B* values of the two observed electronic states (Table 1) means that any transition with $\Delta v_2 > 1$ should be significantly weaker, due to a less favorable Franck–Condon factor.

The evidence of this work also suggests that the vibrational band observed by Fernando et al. [3] at ~11784 cm^{-1} is most likely to correspond to the $\widetilde{A}'^2\Delta_{3/2}(0\,1\,1, \Pi_{1/2}) - \widetilde{X}^2\Sigma^+(0\,0\,0)$ transition of BaOH and the observed vibrational sequence corresponds to the $\widetilde{A}'^2\Delta_{3/2}(01v+1) - \widetilde{X}^2\Sigma^+(00v)$ transitions of BaOH. Based on these assignments and the vibrational frequencies of the low-resolution work (ν'_2 = 342 cm^{-1} and ν'_3 = 468 cm^{-1}) [3], the $\widetilde{A}'^2\Delta_{3/2}(0\,0\,0) - \widetilde{X}^2\Sigma^+(0\,0\,0)$ transition can be approximately calculated to appear at ~10965 cm^{-1}. The $\widetilde{A}'^2\Delta_{5/2}(0\,1\,0, \Pi_{3/2}) - \widetilde{X}^2\Sigma^+(0\,0\,0)$ transition of BaOH can also be estimated from the spin–orbit coupling constant from the $A'^2\Delta$ state of BaF ($A \approx 366$ cm^{-1}) [7]. This procedure predicts the transition to lie at ~11673 cm^{-1}, approximately 189 cm^{-1} to the higher wavenumber side of the previously observed $\widetilde{A}^2\Pi_{1/2}(0\,0\,0) - \widetilde{X}^2\Sigma^+(0\,0\,0)$ transition [4]. Unfortunately no bands were observed in this spectral region during the laser excitation investigation [4], which requires these assignments to be viewed with a degree of caution.

The observed $^2\Pi_{1/2} - \widetilde{X}^2\Sigma^+(0\,0\,0)$ transition of BaOD exhibits a spectral isotopic shift of ~23 cm^{-1} from the BaOH $\widetilde{A}'^2\Delta_{3/2}(0\,1\,0, \Pi_{1/2})$ band. Although this value exceeds a typical spectral shift due to deuteration (e.g. ~6 cm^{-1} for the $\widetilde{A}^2\Pi$ state of SrOH/SrOD [32,33]), it is not unreasonable given the large isotopic shifts of ~53 cm^{-1} observed for the $\widetilde{A}^2\Pi_{1/2}$ sub-states of BaOH/BaOD [5] and ~65 cm^{-1} for the $\widetilde{C}^2\Delta(0\,1\,0) - \widetilde{X}^2\Sigma^+(0\,0\,0)$ transitions of CaOH/CaOD [28]. It therefore seems acceptable to presume that this BaOD band originates from the corresponding vibrational band of the $\widetilde{A}'^2\Delta_{3/2}$ sub-state of BaOH observed in this investigation.

The tentative vibrational assignments for the BaOH and BaOD $\widetilde{A}'^2\Delta_{3/2}(0\,1\,0,\Pi_{1/2}) - \widetilde{X}^2\Sigma^+(0\,0\,0)$ transitions of this study suggest that the $\widetilde{A}'^2\Delta_{3/2}(0\,1\,0,\Pi_{1/2})$ vibronic state is the apparent cause of the perturbations in the previously examined $\widetilde{A}^2\Pi_{1/2}$ $(0\,0\,0) - \widetilde{X}^2\Sigma^+(0\,0\,0)$ transitions. The mixing of these two states has been observed to affect both the spectral positions of their vibrational bands and their rotational structure, (i.e. both global and local perturbations).

The anomalous spin–orbit coupling constants reported for the $\widetilde{A}^2\Pi$ states of BaOH and BaOD [5] are the first indication that this interaction has altered the spectral positions of the observed vibrational bands in the $\widetilde{A}^2\Pi$ and $\widetilde{A}'^2\Delta$ states. This anomaly manifests itself by the differing isotopic shifts in the observed $\widetilde{A}^2\Pi$ and $\widetilde{A}'^2\Delta$ state bands. In particular the $\widetilde{A}^2\Pi_{1/2}(0\,0\,0)$ and $\widetilde{A}'^2\Delta_{3/2}$ $(0\,1\,0,\Pi_{1/2})$ bands exhibit relatively large isotopic shifts and both lie in close proximity with Π vibrational symmetry. This evidence suggests that a Fermi resonance interaction may be the cause of these global perturbations in BaOH/BaOD. Given that no other vibrational bands have been unambiguously assigned for either state it is not possible to deduce the exact magnitude of the perturbation.

Local perturbations are also prevalent in the high-resolution spectra of the $\widetilde{A}^2\Pi(0\,0\,0)$ and $\widetilde{A}'^2\Delta_{3/2}(0\,1\,0,\Pi_{1/2})$ bands of BaOH and BaOD. The apparent failure of the pure precession and unique perturber models in the analysis of $\widetilde{A}^2\Pi$ state [4,5] is a strong indication of perturbations from the closely-lying $\widetilde{A}'^2\Delta$ state. The presence of high-order parameters (e.g. H, A_H, etc.) in the $\widetilde{A}^2\Pi$ state least-squares fit [4,5] also suggests local perturbations are present and caused by a strong interaction between the $\widetilde{A}^2\Pi$ and $\widetilde{A}'^2\Delta$ states. As previously discussed, the least-squares fits generated in the analysis of the two $\widetilde{A}'^2\Delta_{3/2}(0\,1\,0,\Pi_{1/2})$ bands of this work also show evidence of this interaction, yielding large values for p comparable to those seen in the $\widetilde{A}^2\Pi_{1/2}$ state. These observations suggest that perturbations occur between all three low-lying excited electronic states of BaOH and BaOD ($\widetilde{B}^2\Sigma^+, \widetilde{A}^2\Pi$ and $\widetilde{A}'^2\Delta$), which form a mutually perturbing triad, as in BaH and BaD [9].

4.2. The low-lying electronic states

The calculated vertical term energies of Table 2 can further assist in verifying the assignments for the low-lying excited states ($\widetilde{B}^2\Sigma^+, \widetilde{A}^2\Pi$ and $\widetilde{A}'^2\Delta$) of BaOH. The CMRCI vertical term energies for the $\widetilde{B}^2\Sigma^+$ and $\widetilde{A}^2\Pi$ states are both within 80 cm^{-1} of their corresponding experimental values, further verifying the assignments previously proposed [2,4,5]. As only one band of the $\widetilde{A}'^2\Delta$ state has currently been observed by experiment it is difficult to assess the accuracy of the calculated value. However both the experimental and calculated vertical term energies indicate that the $\widetilde{A}'^2\Delta$ state of BaOH should indeed lie below the $\widetilde{A}^2\Pi$ state.

An analysis of the relative barium s, p, and d orbital populations in Table 3 also reveals information on the orbital character of the low-lying electronic states of BaOH. The $\widetilde{B}^2\Sigma^+$, $\widetilde{A}^2\Pi$ and $\widetilde{A}'^2\Delta$ states of BaOH are predicted to originate primarily from excitations to the 5d atomic orbital of barium. Indeed, the state averaged calculations of this work show the $\widetilde{B}^2\Sigma^+$ and $\widetilde{A}'^2\Delta$ states to be primarily derived from the population of the $5d\sigma$ and $5d\delta$ orbitals respectively. In contrast, an analysis of the $\widetilde{A}^2\Pi$ state showed a significant increase in the barium $6p\pi$ orbital population, with its contribution exceeding that of the expected $5d\pi$ orbital. These relative orbital populations were predicted to occur in the $\widetilde{C}^2\Pi$ state, for which the CMRCI calculation yielded a slightly larger $5d\pi$ orbital population (Table 3). This results suggests that the $5d\pi$ and $6p\pi$ orbitals of barium mix strongly in the $\widetilde{C}^2\Pi$ and $\widetilde{A}^2\Pi$ states and both play a significant role in their bonding character.

The $\widetilde{A}^2\Pi$ state of BaOH has recently been reexamined by Frey and Steimle [34] using optical Stark spectroscopy. This investigation yielded electric dipole moments of 1.43 D and 0.477 D for the $\widetilde{X}^2\Sigma^+$ and $\widetilde{A}^2\Pi_{3/2}$ states of BaOH, respectively. Our current CMRCI calculations generated equivalent dipole moments for the $\widetilde{X}^2\Sigma^+$ and $\widetilde{A}^2\Pi$ states of 1.74 D and 1.23 D respectively. A comparison of these values suggests that calculations utilizing a higher level of theory than that implemented in this work are required to accurately reproduce the experimental electric dipole moments for the electronic states of BaOH.

4.3. The higher-lying electronic states

The CMRCI vertical term energy for the $\widetilde{C}^2\Pi$ state (Table 2) is also in good agreement with the experimental value obtained by Pooley et al. [1]. The $\widetilde{D}'^2\Sigma^+$ and $\widetilde{D}^2\Sigma^+$ states both lie at much higher energy and may therefore be expected to require other higher-lying atomic orbitals to be optimized within the active space in order to obtain accurate vertical term energies. Although there are no current experimental data for the $\widetilde{D}'^2\Sigma^+$ state of BaOH, the corresponding $D'^2\Sigma^+$ state of BaF has been observed at ~26227 cm^{-1} [35]. As this is extremely close to the corresponding CMRCI vertical term energy, it seems reasonable that the $\widetilde{D}'^2\Sigma^+$ state of BaOH should lie approximately in this region.

Table 3 indicates that the $\widetilde{D}^2\Sigma^+$ state has primarily s character from the population of the barium $7s\sigma$ orbital, but also shows a small amount of p and d character with the slight increase in both the $6p_z(6p\sigma)$ and $5d_{z2}(5d\sigma)$ orbital populations. This observation is somewhat unexpected as the $\widetilde{D}^2\Sigma^+$ state was thought to originate primarily from a $6p\sigma$ orbital. Furthermore, Table 3 shows that the $\widetilde{D}'^2\Sigma^+$ state arises primarily from the population of the barium $6p\sigma$ orbital with a small amount of mixing from the barium $7s\sigma$ and $5d\sigma$ orbitals. This observation indicates that the $\widetilde{D}'^2\Sigma^+$ and $\widetilde{D}^2\Sigma^+$ states of BaOH are in fact reversed in terms of the atomic orbitals they were thought to originate from.

5. Conclusions

A single band belonging to the $\widetilde{A}'^2\Delta - \widetilde{X}^2\Sigma^+$ band system has been rotationally analyzed for both BaOH and BaOD via V-type double resonance spectroscopy, with the observed spectra mimicking a typical $^2\Pi-^2\Sigma$ transition. Measured rotational lines were assigned and rotational and fine structure parameters determined through a combined least-squares fit with the millimeter-wave pure rotational data of the $\widetilde{X}^2\Sigma^+$ state.

Given the relatively limited observations in this work, it was not possible to unambiguously assign the observed $^2\Pi_{1/2} - \widetilde{X}^2\Sigma^+$ transitions of BaOH and BaOD. However, it seems likely that both bands originate from their corresponding $\widetilde{A}'^2\Delta_{3/2}$ sub-states and may be assigned to a $\widetilde{A}'^2\Delta_{3/2}(0\,1\,0,\Pi_{1/2}) - \widetilde{X}^2\Sigma^+(0\,0\,0)$ transition. These tentative assignments suggest that the vibrational levels of the $\widetilde{A}^2\Pi$ and $\widetilde{A}'^2\Delta$ states of BaOH are in fact interleaved, as in BaF [6].

Complementary *ab initio* calculations were also carried out to investigate the $\widetilde{D}'^2\Sigma^+$, $\widetilde{D}^2\Sigma^+$, $\widetilde{C}^2\Pi$, $\widetilde{B}^2\Sigma^+$, $\widetilde{A}^2\Pi$, $\widetilde{A}'^2\Delta$ and $\widetilde{X}^2\Sigma^+$ states of BaOH. The CMRCI state averaged calculation yielded vertical term energies showing relatively good agreement with existing optical data. Unfortunately, given the approximate manner in which the experimental $\widetilde{A}'^2\Delta$ state term value was estimated, it was not possible to unambiguously conclude which method yielded the more true result. The ambiguity of these assignments may be resolved by adapting the state averaged calculations to yield spin–orbit coupling constants for the $\widetilde{C}^2\Pi$, $\widetilde{A}^2\Pi$ and $\widetilde{A}'^2\Delta$ states of BaOH. Additional *ab initio* investigations may also be used to generate a set of equilibrium geometries and anharmonic vibrational frequencies for the excited electronic states of BaOH. Further calculations to this effect are currently in progress.

Acknowledgments

This research was supported by funding from EPSRC. J.L. thanks the Communauté Française de Belgique (ARC Contract) and the FRS-FNRS (I.I.S.N. project) for financial support. We thank an anonymous referee for suggesting a substantial spin–orbit interaction between the $\widetilde{A}^2\Pi$ and $\widetilde{A}'^2\Delta$ states of BaOH.

Appendix A. Supplementary material

Supplementary data for this article are available on ScienceDirect (www.sciencedirect.com) and as part of the Ohio State University Molecular Spectroscopy Archives (http://library.osu.edu/sites/msa/jmsa_hp.htm). Supplementary data associated with this article can be found, in the online version, at doi:10.1016/j.jms.2011.08.009.

References

[1] S.J. Pooley, M.S. Beardah, A.M. Ellis, J. Electron. Spectrosc. Relat. Phenom. 97 (1998) 77–88.
[2] S. Kinsey-Nielsen, C.R. Brazier, P.F. Bernath, J. Chem. Phys. 84 (1986) 698–708.
[3] W.T.M.L. Fernando, M. Douay, P.F. Bernath, J. Mol. Spectrosc. 144 (1990) 344–351.
[4] J.-G. Wang, J.D. Tandy, P.F. Bernath, J. Mol. Spectrosc. 252 (2008) 31–36.
[5] J.D. Tandy, J.-G. Wang, P.F. Bernath, J. Mol. Spectrosc. 255 (2009) 63–67.
[6] R.F. Barrow, A. Bernard, C. Effantin, J. D'Incan, F. Fabre, A. El Hachimi, R. Stringat, J. Vergès, Chem. Phys. Lett. 147 (1988) 535–537.
[7] C. Effantin, A. Bernard, J. D'Incan, G. Wannous, J. Vergès, R.F. Barrow, Mol. Phys. 70 (1990) 735–745.
[8] A. Bernard, C. Effantin, J. D'Incan, J. Vergès, R.F. Barrow, Mol. Phys. 70 (1990) 747–755.
[9] A. Bernard, C. Effantin, J. D'Incan, F. Fabre, A. El Hachimi, R. Stringat, J. Vergès, R.F. Barrow, Mol. Phys. 62 (1987) 797–800.
[10] R.S. Ram, J. Liévin, P.F. Bernath, J. Mol. Spectrosc. 256 (2009) 216–227.
[11] R.S. Ram, N. Rinskopf, J. Liévin, P.F. Bernath, J. Mol. Spectrosc. 228 (2004) 544–553.
[12] R.S. Ram, J. Liévin, P.F. Bernath, S.P. Davis, J. Mol. Spectrosc. 217 (2003) 186–194.
[13] R.S. Ram, J. Liévin, P.F. Bernath, J. Mol. Spectrosc. 215 (2002) 275–284.
[14] R.S. Ram, A.G. Adam, A. Tsouli, J. Liévin, P.F. Bernath, J. Mol. Spectrosc. 202 (2000) 116–130.
[15] R.S. Ram, J. Liévin, P.F. Bernath, J. Mol. Spectrosc. 197 (1999) 133–146.
[16] R.S. Ram, J. Liévin, P.F. Bernath, J. Chem. Phys. 109 (1998) 6329–6337.
[17] S. Gerstenkorn, J. Verges, J. Chevillard, Atlas du Spectre d'Absorption de la Molecule d'Iode, Laboratoire Aimé Cotton, CNRS II 91405 Orsay, France, 1982.
[18] G. Herzberg, Molecular Spectra and Molecular Structure, vol. 1, Krieger Publishing Company, Malabar, Florida, 1989.
[19] L.M. Ziurys, D.A. Fletcher, M.A. Anderson, W.L. Barclay Jr., Astrophys. J. Suppl. Ser. 102 (1996) 425–434.
[20] M.A. Anderson, M.D. Allen, W.L. Barclay Jr., L.M. Ziurys, Chem. Phys. Lett. 205 (1993) 415–422.
[21] H.-J. Werner, P.J. Knowles, J. Chem. Phys. 82 (1985) 5053–5063;
P.J. Knowles, H.-J. Werner, Chem. Phys. Lett. 115 (1985) 259–267.
[22] H.-J. Werner, P.J. Knowles, J. Chem. Phys. 89 (1988) 5803–5814;
P.J. Knowles, H.-J. Werner, Chem. Phys. Lett. 145 (1988) 514–522.
[23] S.R. Langhoff, E.R. Davidson, Int. J. Quant. Chem. 8 (1974) 61–74.
[24] I.S. Lim, H. Stoll, P. Schwerdtfeger, J. Chem. Phys. 124 (2006) (Article No. 034107).
[25] T.H.J. Dunning, Chem. Phys. 90 (1989) 1007–1023.
[26] R.A. Kendall, T.H. Dunning, R.J.J. Harrison, Chem. Phys. 96 (1992) 6796–6806.
[27] H.-J. Werner, P.J. Knowles, R. Lindh, F.R. Manby, M. Schütz, P. Celani, T. Korona, A. Mitrushenkov, G. Rauhut, T.B. Adler, R.D. Amos, A. Bernhardsson, A. Berning, D.L. Cooper, M.J.O. Deegan, A.J. Dobbyn, F. Eckert, E. Goll, C. Hampel, G. Hetzer, T. Hrenar, G. Knizia, C. Köppl, Y. Liu, A.W. Lloyd, R.A. Mata, A.J. May, S.J. McNicholas, W. Meyer, M.E. Mura, A. Nicklaß, P. Palmieri, K. Pflüger, R. Pitzer, M. Reiher, U. Schumann, H. Stoll, A.J. Stone, R. Tarroni, T. Thorsteinsson, M. Wang, A. Wolf, MOLPRO 2008, Version 2008.1.
[28] C.N. Jarman, P.F. Bernath, J. Chem. Phys. 97 (1992) 1711–1718.
[29] H. Lefebvre-Brion, R.W. Field, The Spectra and Dynamics of Diatomic Molecules, Elsevier, Academic Press, San Diego, 2004 (Private Communication).
[30] J.M. Brown, A.S-C. Cheung, A.J. Merer, J. Mol. Spectrosc. 124 (1987) 464–475.
[31] G. Herzberg, Molecular Spectra and Molecular Structure, vol. 3, Krieger Publishing Company, Malabar, Florida, 1991.
[32] C.R. Brazier, P.F. Bernath, J. Mol. Spectrosc. 114 (1985) 163–173.
[33] S. Yu, J.-G. Wang, P.M. Sheridan, M.J. Dick, P.F. Bernath, J. Mol. Spectrosc. 240 (2006) 26–31.
[34] S.E. Frey, T.C. Steimle, Chem. Phys. Lett. 512 (2011) 21–24.
[35] K.P. Huber, G. Herzberg, Molecular Spectra and Molecular Structure, vol. 4, Van Nostrand Reinhold, New York, 1979.